DIMITRI

D2:ATBD RADIOMETRY MONITORING OVER DCC

TECHNICAL NOTE

	Name	Company	Date	Signature
Prepared by :	B. Berthelot	Magellium	25/12/2020	
Checked by :	B. Alhammoud	Argans	29/03/2021	
Approved by :	M. Bouvet	ESA		

Document reference :	RFQ-QA4EO-DIMITRI-TN-010-MAG_ATBD-DCC
Issue.Revision :	1.0
Date :	25/12/2020
Client :	ESTEC
Ref., Tender :	QA4EO - DIMITRI evolution

Distribution list

	Name	Company	N. copies
Addresses :	M. Bouvet B. Alhammoud	ESA/ESTEC Argans	1
Internal copy :	Customer file Project Manager Development team	Magellium Magellium Magellium	1 (digital) 1 (digital) 1 (digital)

Document Change Record

Iss.	Rev.	Date	Reason	Comments
1	0	25/12/2020	Creation of the document	
1	4	29/03/2021	Results Update with 2017 OLCI-A acquisitions	

Table of contents

List of the Tables

List of the Figures

1 Objectives of the document

The purpose of this study is to develop and implement a method to monitor sensor radiometry of optical sensors using DCC into DIMITRI software.

1.1 Related documents

1.1.1 Applicable documents

Table 1-1: List of applicable documents

Id.	Ref.	Description
AD1	QA4EO-QAEO-GEN-DQK-001/7, Version 4.0	QA4EO Guidelines (seven documents) http://qa4eo.org/
AD2	Statement of Work 'QA4EO DIMITRI Evolution'	TEC-EEP/2015.23/MB, Issue 1, Rev. 6, 15 April 2015

1.1.2 Reference documents

Table 1-2: List of reference documents

Id.	Ref.
RD 1.	R - 10: Fougnie B. Bach R., Monitoring of Radiometric Sensitivity Changes of Space Sensors Using Deep Convective Clouds: Operational Application to PARASOL, IEEE TRANSACTIONS ON GEOSCIENCE AND REMOTE SENSING, VOL. 47, NO. 3, MARCH 2009

1.1.3 Bibliography

- E. F. Vermote and Y. J. Kaufman, "Absolute calibration of AVHRR visible and near infrared channels using ocean and cloud views," Int. J. Remote Sens., vol. 16, no. 13, pp. 2317–2340, 1995.
- B. Lafrance, O. Hagolle, B. Bonnel, Y. Fouquart, and G. Brogniez, "Interband calibration over clouds for POLDER space sensor," IEEE Trans. Geosci. Remote Sens., vol. 40, no. 1, pp. 131–142, Jan. 2002.
- Hu, Y., B. Wielicki, P. Yang, P. Stackhouse, B. Lin, and D. Young, Application of deep convective cloud albedo observations to satellite-based study of terrestrial atmosphere: monitoring stability of space-borne measurements and assessing absorption anomaly. IEEE Trans. Geosci. Remote Sensing, 2004.
- Bhatt, R.; Doelling, D.R.; Wu, A.; Xiong, X.; Scarino, B.R.; Haney, C.O.; Gopalan, A. Initial Stability Assessment of S-NPP VIIRS Reflective Solar Band Calibration Using Invariant Desert and Deep Convective Cloud Targets. Remote Sens. 2014, 6, 2809-2826.

- Doelling, D.R.; Nguyen, L.; Minnis, P. On the use of deep convective clouds to calibrate AVHRR data. Proc. SPIE 2004, doi:10.1117/12.560047.
- Doelling, D.R.; Hong, G.; Morstad, D.L.; Bhatt, R.; Gopalan, A.; Xiong, X. The characterization of deep convective cloud albedo as a calibration target using MODIS reflectances. Proc. SPIE 2010, doi:10.1117/12.869577.
- Doelling, D.R.; Morstad, D.L.; Scarino, B.R.; Bhatt, R.; Gopalan, A. The characterization of deep convective clouds as an invariant calibration target and as a visible calibration technique. IEEE Trans. Geosci. Remote Sens. 2013, 51, 1147–1159.
- VITO, PROBA-V Image Quality Center (IQC) ATBD, 2013.
- Sterckx et al. 2014, The PROBA-V mission: image processing and calibration, International Journal of Remote Sensing, 35:7, 2565-2588, DOI: 10.1080/01431161.2014.883094
- Monitoring of Radiometric Sensitivity Changes of Space Sensors Using Deep Convective Clouds: Operational Application to PARASOL
- Fougnie, B., and R. Bach, Monitoring of radiometric sensitivity changes of space sensors using Deep Convective Clouds - Operational application to PARASOL, IEEE Trans. Geosci. Remote Sens., 47(3), 851-861, 2009.
- Lamquin et al., 2020, OLCI A/B Tandem Phase Analysis, Part 3:Post-Tandem Monitoring of Cross-Calibration from Statistics of Deep Convective Clouds Observations, Remote sensing.
- C. Emde, R. Buras-Schnell, A. Kylling, B. Mayer, J. Gasteiger, U. Hamann, J. Kylling, B. Richter, C. Pause, T. Dowling, and L. Bugliaro. **The libradtran software package for radiative transfer calculations (version 2.0.1).** *Geoscientific Model Development*, 9(5):1647-1672, 2016

1.1.4 Acronyms

6SV	Second Simulation of a Satellite Signal in the Solar Spectrum, Vector
AATSR	Advanced Along Track Scanning Radiometer
ADEOS	Advanced Earth Observation Satellite
ATSR	Along Track Scanning Radiometer
ATBD	Algorithm Theoretical Basis Document
BRDF	Bidirectional Reflectance Distribution Function
Cal/Val	CALibration and VALidation
CCN	Contract Change Notice
CEOS	Committee on Earth Observation Satellites
CNES	Centre National d'Etudes Spatiales
DB	Database
DCC	Deep Convective Cloud
DIMITRI	Database for Imaging Multi-spectral Instruments and Tools for Radiometric Intercomparison
DN	Digital Number
ECMWF	European Centre for Medium-Range Weather Forecasts
ENVISAT	ENVIronment SATellite
EO	Earth Observation
ESA	European Space Agency
EUMETSAT	European Organisation for the Exploitation of Meteorological Satellites

GSICS	Global Space-based Inter-calibration System
GSP	General Study Programme
GUI	Graphic User Interface
IDL	Interactive Data Language
IVOS	Infrared and Visible Optical Sensors
LUT	Look Up Table
MERIS	Medium Resolution Imaging Spectrometer
MODIS	Moderate Resolution Imaging Spectroradiometer
MSI	MultiSpectral Imager
NASA	National Aeronautics and Space Administration
NOAA	National Oceanic and Atmospheric Administration
OLCI	Ocean and Land Color Instrument
PARASOL	Polarization & Anisotropy of Reflectances for Atmospheric Sciences coupled with Observations from a Lidar
POLDER	POLarization and Directionality of the Earth's Reflectances
QA4EO	Quality Assurance Framework for Earth Observation
RTM	Radiative Transfer Model
S-2 / S-3	Sentinel 2/3
SLSTR:	Sea Land Surface Temperature Radiometer
SUM:	Software User Manual
SW:	Software
SWIR	Short Wave Infra-Red
TOA	Top Of Atmosphere
VGT	VEGETATION
VIS	VISible
WG	Working Group
WGCG	Working Group on Calibration and Validation

2 Introduction

This Algorithm Theoretical Basis Document describes the algorithm used to monitor the multitemporal calibration of satellite sensors using Deep Convective Clouds (DCC). In particular, this document identifies sources of input data, both satellite and auxiliary data. It provides the physical theory and mathematical background underlying the use of this information in the method. It includes implementation details, and describes assumptions and limitations of the adopted approach.

This task is referred by WP 500.1 and WP 500.2 of the SOW.

It is applied to DCC extracted from S3A/OLCI instrument.

Section 3 outlines the baseline DCC calibration technique applicable to most operational visible sensors.

Section 4 details the method and its implementation. Results obtained for S3A/OLCI instruments are given in section 5. Section 6 recaps the uncertainty of the method.

3 Bibliography review

DCC are used to monitor the stability of sensor radiometry because they are pseudo invariant such as deserts and oceanic sites are. These clouds are located in the tropopause, meaning that the part of signal coming from the atmosphere at sensor level is reduced over these targets (except if there are no stratospheric aerosols). In particular, radiative impact of atmospheric water vapor absorption, aerosols, and surface albedo is minimal. They are highly reflective and have predictable near Lambertian albedos. DCCs exhibit a nearly flat spectral response. They are identified using a threshold based method.

DCC calibration techniques are statistical based methods. They have been developed a long time ago. The pioneers were probably Vermote and Kaufman in 1992 who used DCCs to monitor the inter band calibration of AVHRR VIS and NIR bands. Since, efforts have been made to characterize and model the variability of DCC in order to monitor the trends of calibration gain using different methodologies.

Two families of methods are commonly used. The ones relying on the measurement prediction using RTM able to simulate cloud reflectances. The others using statistics based methods using a large collection of measurements (> 100000). The following sections provides some references for both types of methodologies.

3.1 Overview of methods using RTM

3.1.1 AVHRR (Vermote and Kaufman, 1992)

30 years ago, Vermote and Kaufman (1992) developed a method used to derive AVHRR intercalibration using bright clouds. Considering that the spectral variability of DCC is low below 1 µm and that clouds can be considered as lambertian for SZA close to nadir, the differences between VIS and NIR channels of AVHRR are directly related to the instrument stability. The authors used the DCC to transfer the calibration of AVHRR 0.65 µm band to the 0.86 µm band by assuming that the reflectance ratio was constant for BTs less than 225 K.

The authors provided an error budget accounting for the assumption of cloud isotropy, the aerosol and water vapour, Rayleigh correction, ozone and oxygen correction. It leads to the overall uncertainty of 2%.

3.1.2 Proba V (Sterckx et al., 2014)

Sterckx et al., 2014 have developed a relative radiometric calibration method using DCC for Proba V sensor. The method has been described in Lafrance et al. 2002, Sohn et al. (2009). They used B2 (red) band as reference band to inter calibrate B0 (Blue) and B3 (NIR) bands. The method is not suited for the SWIR band as the reflectance is no longer invariant over this spectral region.

The method consists in predicting the TOA reflectance in the reference band using a radiative transfer code which simulates the reflectance over clouds. Adjustment consists in estimating the cloud optical thickness which allows to simulate the TOA reflectance in the reference band and transfer it to another band to evaluate the accuracy of interband calibration coefficients. Measurements are corrected for ozone absorption.

As the use of the RTM (Libradtran) is not possible due to excessive computation time, they build a LUT of TOA reflectances for different cloud characteristics.

Cloud scattering properties are taken from Baum et al. 2005 and are used to specify cloud optical properties in the RTM. They consider clouds as nonspherical ice particles. The cloud-top and cloud-base heights are assumed to be 15 and 1 km, respectively, resulting in a geometric thickness of 14 km.

DCC pixels are selected based on a sequence of five tests: (1) a geometry test to reject observations corresponding to viewing geometries near the specular direction; (2) a cloud-land distance test; (3) a NIR reflectance test: a thresholding test is done on the NIR values, as NIR values below the threshold are not strong enough to derive reliable results; (4) a homogeneity test to check if values are sufficiently homogeneous over the samples to derive reliable results and (5) a cloudy neighborhood test to check if the pixel neighborhood is cloudy. If not, the pixel is masked, to avoid influences from non-cloudy pixels.

Inter band calibration results for Blue and NIR bands and for each camera (with respect to reference band) are shown in the figure below, showing the stability of the NIR cameras.

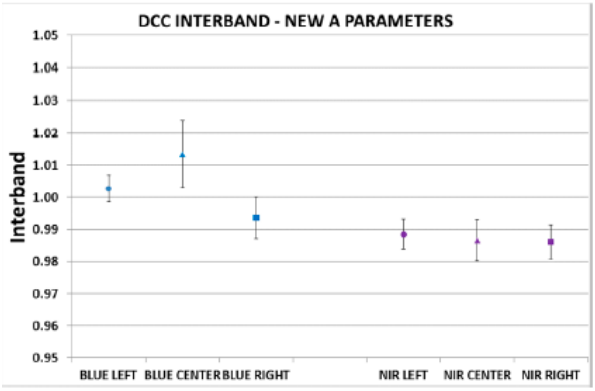

Figure 3-1: Inter-band Deep Convective Cloud (DCC) results, relative to the RED reference band with the vicariously updated calibration.

Sterckx and al. (2014) performed a sensitivity error by performing simulations where inputs are modified against the chosen reference. The error analysis is reported in the table below.

Table 3-1: Calibration error budget for DCC

Error sources	Average error (%) in the BLUE channel	Average error (%) in the NIR channel
Cloud effective radius (10 µm)	0.300	0.886
Microphysical model	0.218	0.758
Cloud top height	0.095	0.011
Cloud geometrical depth	0.040	0.002
Ozone (20%)	0.359	0.397
Atmospheric profile	0.003	0.001
Red calibration error (3%)	2.912	2.704
Total interband	0.526	1.231
Total absolute	2.959	2.971

3.1.3 PARASOL (Fougnie and Bach, 2009)

Fougnie and Bach (2009) developed a method for inter band calibration applied to PARASOL sensor. Modeling uses the reference band (670 nm) to invert the cloud optical thickness assuming a type of cloud top particles, and computes for other bands (490 to 865 nm) the reflectance to be compared with the satellite sensor measurement through a radiative transfer look-up-table.

The transfer of the calibration in the red to blue and the near infrared is accurate, and allows an absolute calibration in this spectral range, complementing other calibration methods (Rayleigh, sun glint).

The use the Discrete Ordinates code (Stammes et al, 1988) to simulate the cloud reflectance assuming a vertical description of the cloud and atmosphere divided into 16 layers, and for which cloud particle type, aerosol type, and optical thickness are defined according Lafrance et al. (2002).

Fougnie and Bach, 2009, provide an error budget for COT, molecular and aerosol scattering contributions, surface contribution and gaseous contribution, reported in the table below.

Table 3-2: Typical error budget for the inter-band calibration method over clouds in % (from Fougnie and Bach, 2009)

Error type	443	490	565	765	865
Cloud particle model (microphysics)	**2.19**	1.01	0.73	0.47	**2.33**
Cloud top altitude (3 km)	0.69	0.42	0.18	0.07	0.11
Aerosol (100% on stratospheric AOT)	0.14	0.09	0.05	0.02	0.04
Gas amount (20% for O_3/O_2)	0.39	0.19	0.81	0.95	0.34
RMS	2.33	1.12	1.11	1.06	2.36

It shows that for the 490, 565 and 765 nm spectral bands, close to the 670 nm reference band, the error due to cloud microphysics is very small (less than 1%). Others error types are less than 1% leading to the RMS performance around 1%.

3.2 Overview of methods using only statistics

3.2.1 VIIRS, (Doelling et al., 2013)

First developed by Hu et al, 2004 for CERES and MODIS sensors, the method is a statistical approach that relies on the assumption that the distribution of DCC reflectance remains constant over time. Doelling et al. (2004) used also the approach for AVHRR and later for MODIS (2013) and VIIRS (2014).

The DCCs are identified using only IR temperature and spatial uniformity thresholds and angular constraints to capture the most lambertian part of DCC. Anisotropic corrections are added to corrected DCC reflectances (Hu et al, 2004). DCC pixels are collected and used to construct monthly probability distribution functions (PDFs) to monitor sensor stability. The monthly PDF modes and means are linearly regressed to derive the stability of the sensor.

Figure 3-2 illustrates the method used to monitor the VIIRS M5 channel stability. 200,000 DCC pixels have been identified every month to compute the monthly PDFs of the normalized DCC

radiances. The statistical mean and mode are computed for each monthly PDF, and are tracked over time to monitor the stability of the instrument. Statistics are given in Figure 3-2 (right)

In this case, the stability of the VIIRS M5 channel is found to be 0.39%/yr using the mean and −0.16%/yr using the mode.

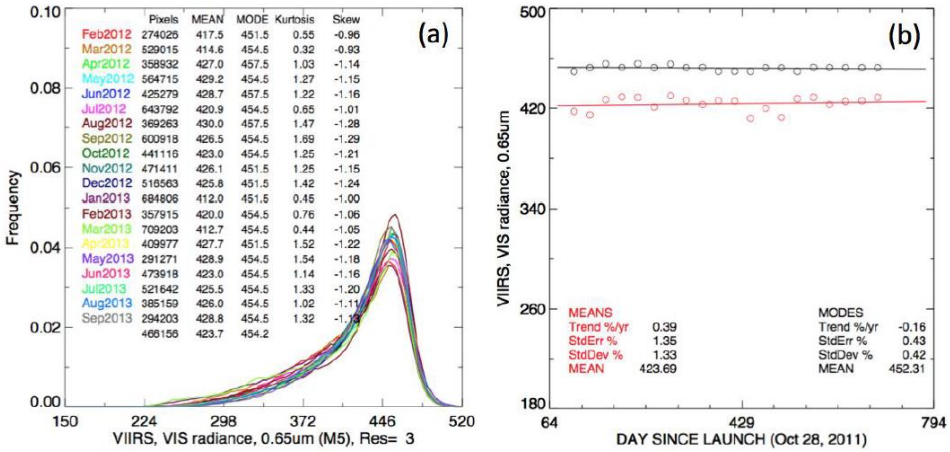

Figure 3-2: (a) The VIIRS M5 channel DCC monthly PDFs over the Tropical West Pacific (TWP) domain; and (b) the corresponding PDF mode and mean radiance trends showing the stability of the sensor. The ADM normalized radiance units are in $W{\cdot}m^{-2}{\cdot}sr^{-1}{\cdot}\mu m^{-1}$.

3.2.2 OLCI, (Lamquin, et al. 2020)

Lamquin et al, 2020 described a method to monitor OLCI/A and OLCI/B intercalibration using DCC observations. Instead of using the mode or the mean as Doelling et al. (2013) did, they monitor the inflexion point of DCC reflectance distributions as an indicator of the absolute calibration for each subdivision of the OLCI Field-of-View. TOA reflectances are corrected from gaseous absorption. Ratios of DCC reflectances provide the interband calibration.

Inflexion points from Pdfs for samples containing 5000 observations are plotted in the figure below.

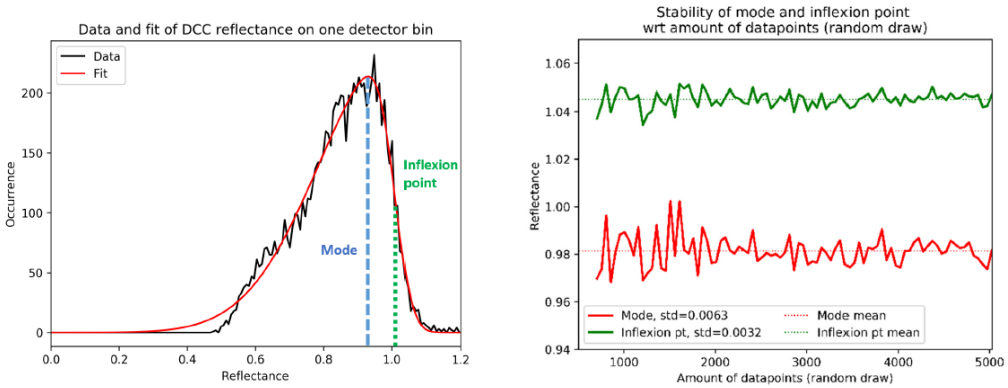

Figure 3-3: (left) Example of probability distribution function of the DCC reflectance (black line) from OLCI DCC observations along with its fit using a skewed-gaussian function (red line).Right image, Mode (red) and inflexion point (green) values obtained over iterative sub-samples of random DCC observation samples of increasing number of data points as function of this number (Source Lamquin et al, 2020).

4 Algorithm overview

4.1 Principle of the method

In the method, we account for DCC characteristics and reflective properties (spectral, directional) already reported in the previous section to develop a method which principle is to compare the measurements provided by the sensor above the DCC site to a simulation of the top-of-atmosphere reflectance (Eq. 1). This ratio is computed for all acquisitions and monitored on a large period of time to detect possible change in sensor radiometry.

$$\Delta\rho = \frac{\rho_{TOA}^{Measured}}{\rho_{TOA}^{Simulated}} \quad \textbf{Eq. 1}$$

In this ATBD, we will describe the method implemented to monitor the temporal variability of this ratio.

Main characteristics of DCCs

Tropical deep convective clouds are an excellent invariant target for vicarious calibration of satellite visible (VIS) and near-infrared (NIR) solar bands. DCC TOA reflectances are spectrally flat in the visible and NIR. The tropics are active regions for deep convective cloud formation. These clouds are located over ocean. They are large and bright, and their top is located above 10 km. Therefore, the TOA reflectances measured over these clouds depends on the cloud reflectance and the ozone transmission, and less of the molecular scattering and aerosol scattering.

4.1.1 Method

DCC calibration method relies on the comparison between TOA reflectances (corrected for gaseous absorption) measured by the sensors (in our case OLCI/S3A) available in DIMITRI database and the modelled TOA reflectances.

The DCC radiometry monitoring is based on the monitoring of the stability of ρ_{toa}. A model simulating radiative transfer into Cloud is used to simulate cloud TOA reflectance. ,

Let's call $\rho_{TOA}^{Measured^*}$ the apparent Top Of Atmosphere reflectance, and $\rho_{TOA}^{Measured}$ the TOA reflectance.

The DCC reflectance in VIS and NIR spectrums is mainly a function of cloud optical depth. The apparent TOA reflectance, normalised to the gaseous transmission, is modelled by the following expression:

$$\rho_{toa}^{Measured} = Tg.\rho_{dcc}(\tau_c + \tau_a + \tau_r) \quad \textbf{Eq. 2}$$

and

$$\rho_{TOA}^{Measured} = \frac{\rho_{TOA}^{Measured^*}}{Tg} \quad \textbf{Eq. 3}$$

Where Tg is the total gaseous transmission, ρ_{DCC} the reflectance at the top of the cloud/atmosphere system and τ_c, τ_a, and τ_r are respectively the clouds, aerosol and Rayleigh optical thickness in the different atmospheric layers.

The comparison of the modelled to the measured reflectance over time provided the assessment of the sensor radiometry.

In the method, the TOA reflectance values are estimated using libRadtran RTM (Emde et al., 2016). In this case, simulated TOA reflectances values are determined by three types of factors:

- cloud properties
- atmospheric conditions

  Aerosol loadings are unknown. A mean value of 0.05 is be used.
- Surface conditions
- Observation conditions including solar zenith angle, view zenith angle and relative azimuth angle.

4.1.2 RTM Model

We choose to use Libradtran RTM to perform the simulations for all spectral bands of the sensor, the geometrical illumination and observation conditions, an atmosphere described by an aerosol model and an optical thickness, an atmospheric profile depending on the latitude, no absorption, a cloud optical thickness and a water leaving reflectance.

The method is based on the use of Look Up Tables containing simulated TOA reflectances for a large range of variations of the inputs parameters and the search the actual configuration which is closest to the simulation.

4.2 Implementation description

4.2.1 Overall steps

This paragraph provides with the overall steps that have to be done to estimate the ratio of measured to simulated reflectance.

1) Read the *database* and select images containing DCC.

   For each selected date (loop)

2) Read the TOA reflectances for the selected date.
3) Read auxiliary data
   3.1) Ozone content
4) Check Pixels selection test
   4.1) Select dcc pixels
5) Correct the measured TOA reflectances from ozone gaseous absorption
6) Find the COT in red band (B7 for OLCI)
7) Estimate the reflectance ratio $\Delta\rho = \frac{\rho_{TOA}^{Measured}}{\rho_{TOA}^{Simulated}}$ in the all bands

4.2.2 Detailed steps

4.2.2.1 Input data selection

DIMITRI data ingestion module allows to extract for each acquisition the area which contains the DCC target site. One file is written for one acquisition. According to the period selected by the user, these files are read and used as input of the method.

The output file of the ingestion module contains the following information:

- Latitude;
- Longitude;
- Zenith and azimuth solar angles;
- Zenith and azimuth view angles;
- TOA reflectances in all channels;
- Cloud mask ;

4.2.2.2 Auxiliary data extraction

Ozone content is provided from metadata inside the products.

4.2.2.3 Pixel selection

The selection of DCC pixels is the first step of the processing.

- Deep convective clouds develop over subtropical warm oceans in inter-tropical. Latitudes between 30°N and 30°S are selected
- remove all pixels or which solar zenith angles > 40° or viewing zenith angles > 30° to avoid possible shadowing effects and take advantage of the more Lambertian part of the DCC reflectance field
- use only pixels for which relative azimuth is between 30 and 150° to reject observations corresponding to viewing geometries near the specular direction.
- remove selection if ref(B1|B2|B3|B16|B17|B18) < 0.8 to ensure that thick clouds are selected
- Spatial homogeneity σ < 3% inside a 3 x 3 window, to select only homogenous convective core of the clouds

4.2.2.4 Correction of the apparent TOA reflectance from gaseous transmission

The comparison of the measured reflectance to the estimated one is performed on apparent TOA reflectances corrected from the gaseous transmission. Therefore, it is necessary to estimate the ozone gaseous transmission for each pixel selected by the previous selection step.

The gaseous transmission for ozone has been estimated using SMAC formulation.

- Input for total gaseous transmission estimation is :
  - Solar zenith angle
  - View zenith angle
  - Ozone content
  - SMAC coefficients for all bands
- Output is :
  - Ozone gazeous transmission.

4.2.2.5 COT estimation in the reference band

This estimation is an important step of the method. The algorithm estimates the COT using the LUT of the reference spectral band such as the simulated TOA reflectance is equalled to the observed one. Then, the COT is used to estimate the TOA reflectance that should be measured in the other bands.

The reference band for S3A is the band 7 centered at 620 nm.

4.2.2.6 TOA reflectance estimation

Libradtran is used to simulate the TOA reflectance (normalised to the gaseous transmission) using the atmosphere characteristics and the solar and view geometry of the acquisition.

4.2.2.7 $\Delta\rho$ estimation in the all bands

The ratio of measured TOA reflectances out to simulated TOA reflectances is computed for all the bands.

$$\Delta\rho = \frac{\rho_{toa}^{measured}}{\rho_{toa}^{estimated}} \quad \textbf{Eq. 4}$$

As the algorithm is applied on a pixel per pixel basis, a statistical analysis on the ratio is made to remove outliers. Mean and standard deviation of the ratio are estimated and values out of three σ are removed.

4.2.2.8 Statistical analysis of the sensor radiometry

The last step consists in averaging the values of the ratio obtained for one acquisition and monitor it with time.

$$\overline{\Delta\rho} = mean\left(\frac{\rho_{TOA}^{Measured}}{\rho_{TOA}^{Simulated}}\right) \quad \textbf{Eq. 5}$$

4.2.3 Auxiliary data

4.2.3.1 Generation of LUTS

To apply the method, Look Up Tables are computed using the libradtran RTM (Emde et al, 2016). Disort is the solver. Band parameterization with a spectral resolution of 15 cm^{-1} is used.

4.2.3.1.1 Constants

The selected **atmospheric profile** for the simulations is tropical atmosphere.

No gaseous absorption

The choice of the **aerosol model** is the maritime model from OPAC 98% humidity.

A **mean aerosol optical thickness (AOT)** of 0.05 at 550 nm is used to generate the LUT.

Top cloud height is 15 km, with a basis located at 1km.

Liquid water is set to 0.015 g/m3 at the bottom of the cloud.

4.2.3.1.2 Look Up tables

The TOA reflectance corrected from gaseous transmission is computed for a set of varying input for each spectral used in the processing. This LUT is a function of sun zenith angle, view zenith angle, relative azimuth angle, and COT.

Libradtran v2.0.3 is used because it accounts for cloud phase, micro-physical properties as well as a complete description of the background atmosphere and surface. Both water and ice clouds models are included. The microphysical properties of water clouds are converted to optical properties either according to the Hu and Stamnes (1993) parameterization or by Mie

calculations. For the optical properties of ice clouds calculations from Baum et al. (2005) are used.

As cloud reflectance for the VNIR bands is rather insensitive to the effective particle radius, the effective radius is assumed fixed for the calibration. According to Sohn et al. 2009 MODIS effective particle radii for DCCs from one month of data show a narrow distribution with maximum frequency at 20 µm. LUT calculations will be performed for an effective radius of 20 µm.

Grid points of the LUT are:

- SZA : 9 to 41 °, with a step of 2°
- VZA : 0 to 30° °, with a step of 2°
- Dphi : 0 to 180 °, with a step of 30°
- COT: 20 to 200 with a step of 5

Remark: The cloud spectral properties are only available from 400 nm. For OLCI, this means that simulations can not be performed for band 1.

5 Dataset analysis to monitor the sensor radiometry using DCC targets

5.1 Introduction

This section illustrates the automatic selection of the DCC in 548 S3A acquisitions over the Maldives. These images have been ingested by DIMITRI tool (Figure 5-1). They are provided in netcdf format.

All the images have been acquired with the VZA between 10 and 30° and 45 and 60°. The SZA varies with time of acquisition between 25 and 55°. Mean TOA reflectances of the scenes are lower than 0.8.

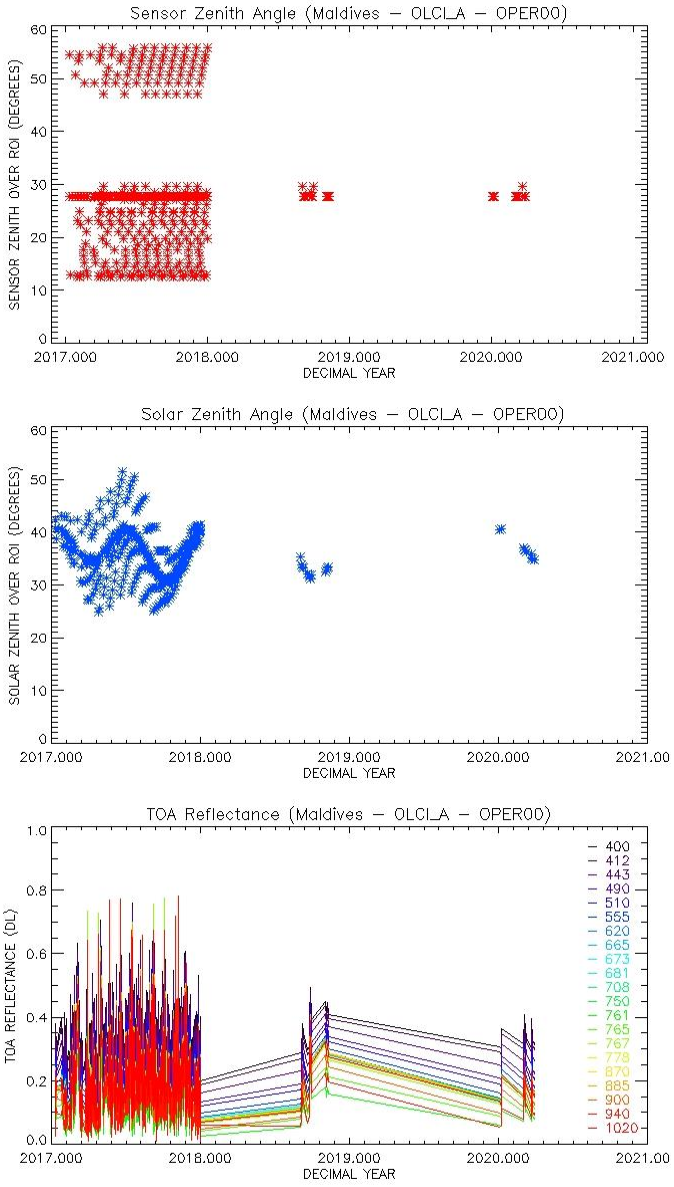

Figure 5-1: Dimitri dataset characteristics

5.2 DCC identification

According to the pixel selection applied to the images, the DCC pixels identified are represented on the following plots. Triplets of images are the NIR reflectances, the cloud mask (created at the ingestion) included the DCC location, the reflectance of DCC.

An example is given for the acquisition of 2018-11-08

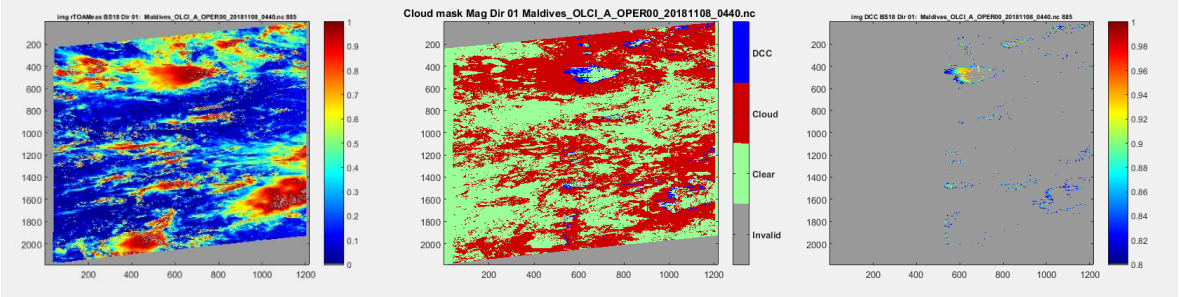

Figure 5-2: Mask of DCC (left images), Mask of cloud details (middle), NIR TOA reflectance (right images)

5.3 Analysis of the saturation of S3A/OLCI in identified DCCs

As observed on the images of DCC identification, there are no large compact DCC identified due to reflectance saturation. An example taken from 08/11/2018 images (Figure 5-3) details the saturation of TOA reflectance on all channels (Figure 5-4).

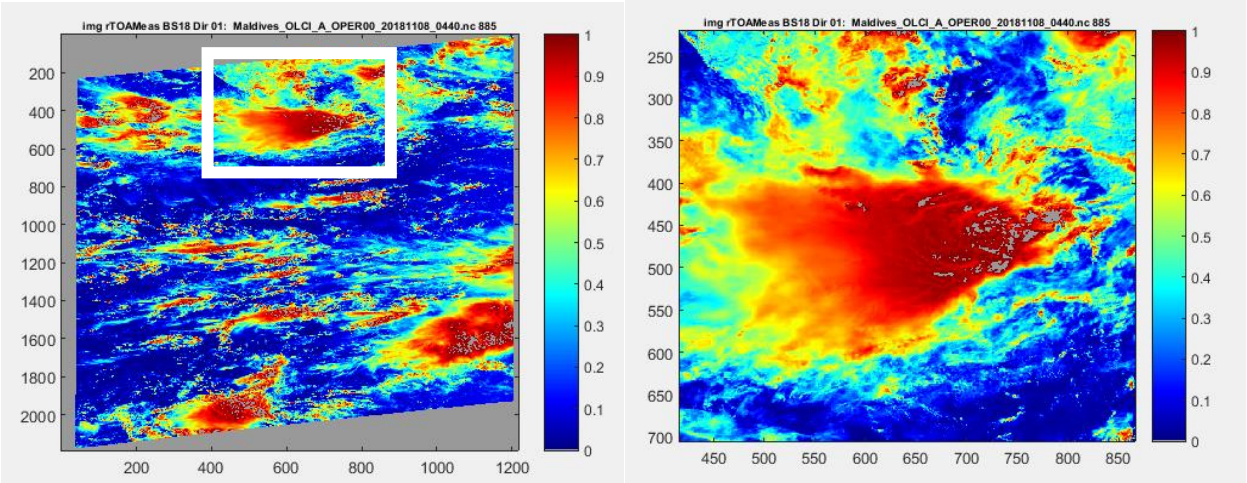

Figure 5-3: NIR TOA reflectance (right image), DCC (right image)

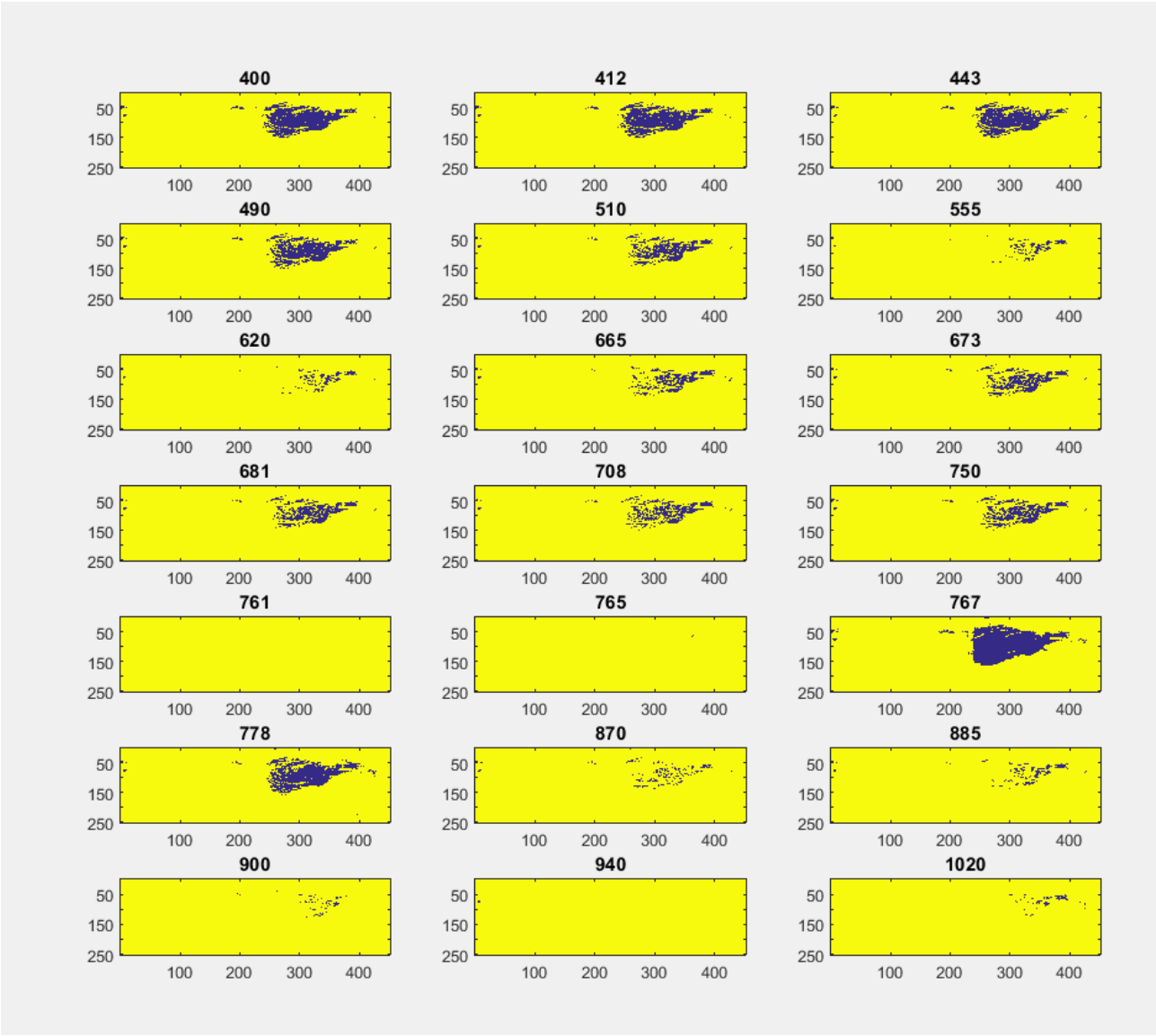

Figure 5-4: Pixels flagged as invalid in all S3/OLCI channels

For the identified clouds, the saturation is highligted on Figure 5-5.

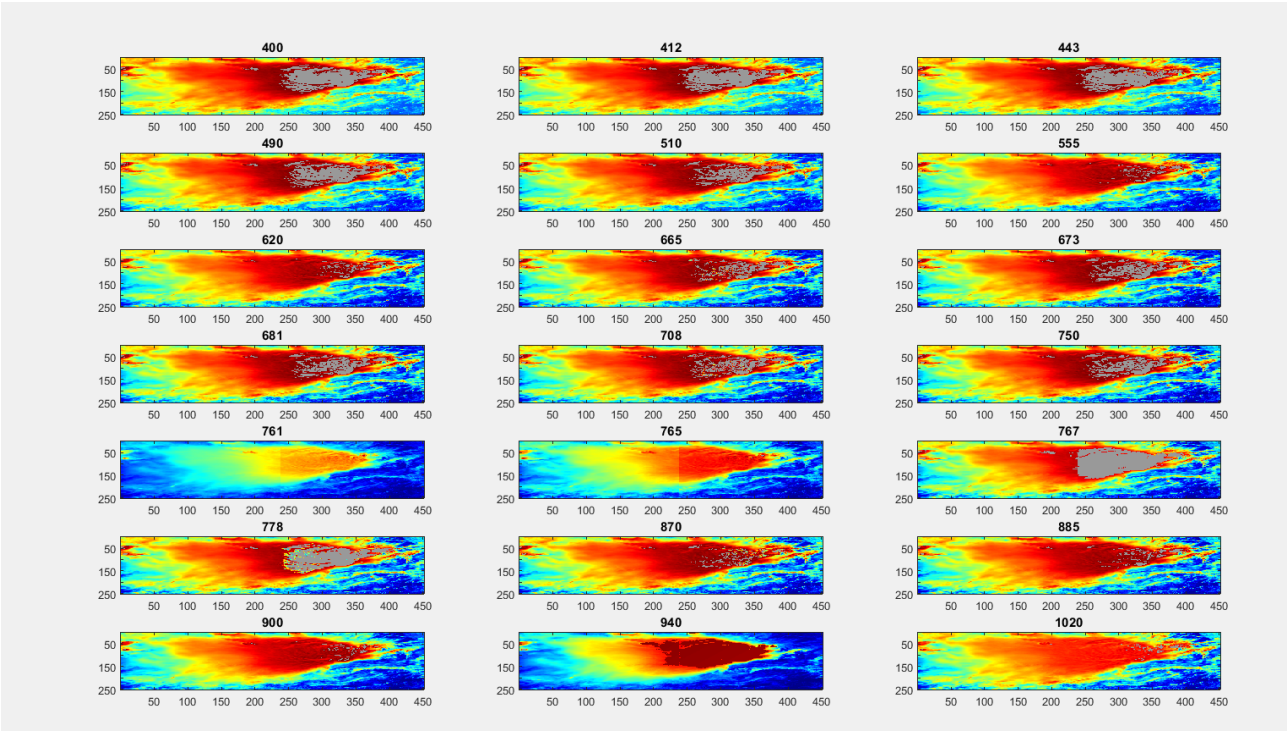

Figure 5-5: TOA reflectances over the identified DCC

At the end of the pixel selection method which combines several channels, the mask of DCC is represented in the figure below. Large area inside the DCC are not usable for calibration due the saturation.

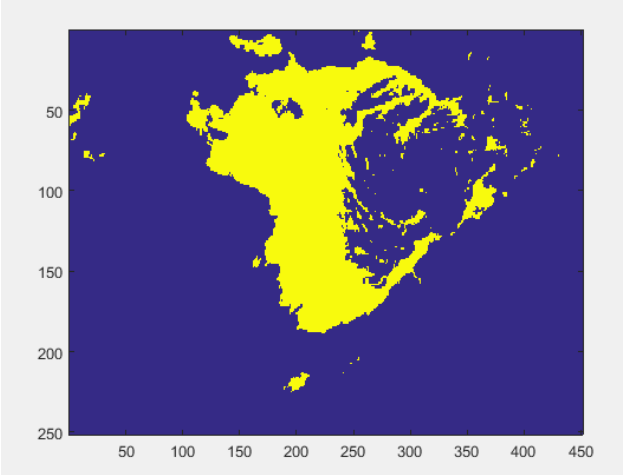

Figure 5-6: Mask of DCC

6 Results

6.1 For a date

The results are detailed for an OLCI_A acquisition dated on 01/11/2018 where three cloudy masses are visible on the image.

Figure 6-1: Quicklook of the acquisition.

The DCC detection is applied on the image and provides the following mask. DCC pixels are identified in blue color. The TOA reflectances of the DCC are indicated on the image on the right.

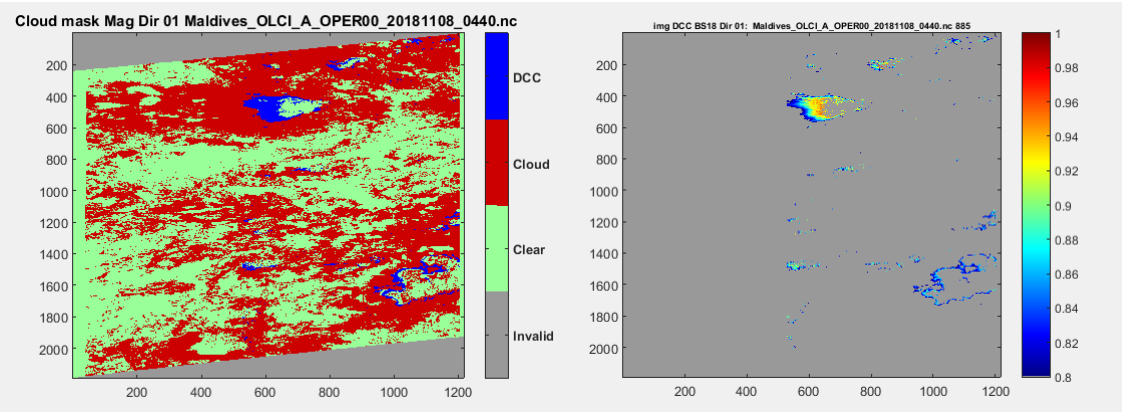

Figure 6-2: DCC location on the left; TOA reflectance in the NIR on the right.

The ratio of measured to simulated TOA reflectances is reported in the figures below for all bands except 940 nm. Results are presented for four cases:

1) Case 1: When no filtering is applied
2) Case 2: When a filtering of the outliers at 3 sigma is applied
3) Case 3: When DCC pixels are selected in a compact area of 3 x 3 km2.
4) Case 4: When DCC pixels are selected in a compact area of 3 x 3 km2 and post filtering applied.

No Filtering	Ratio filtered at 3 sigma	DCC detection using 3 km2 filled kernels	DCC detection using 3 km2 filled kernels. Ratio filtered at 3 sigma
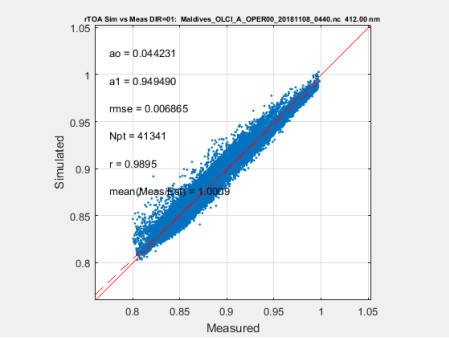	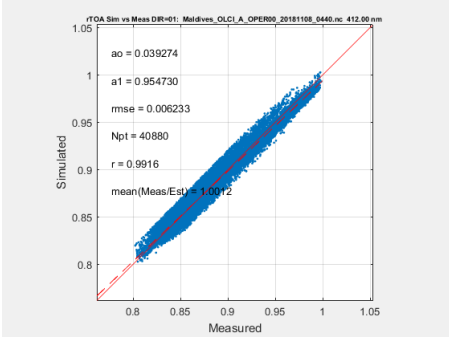	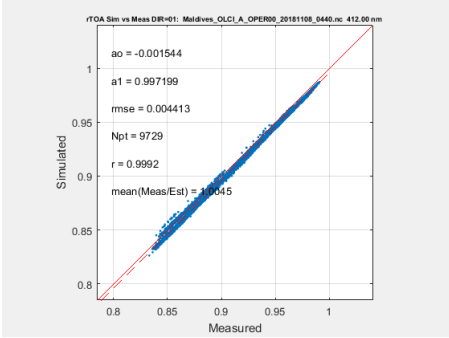	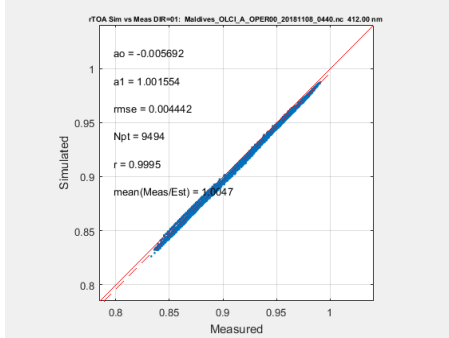
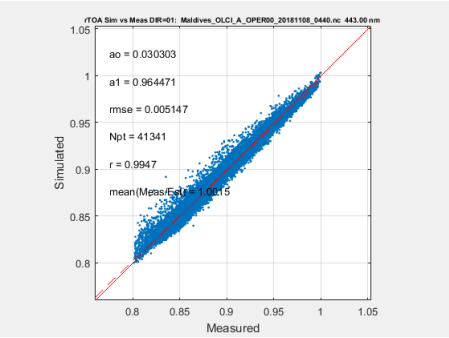	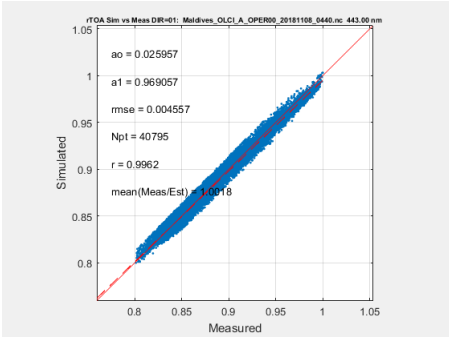	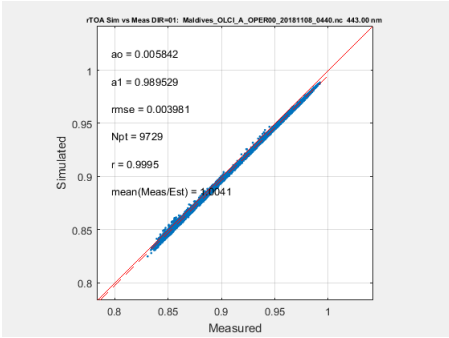	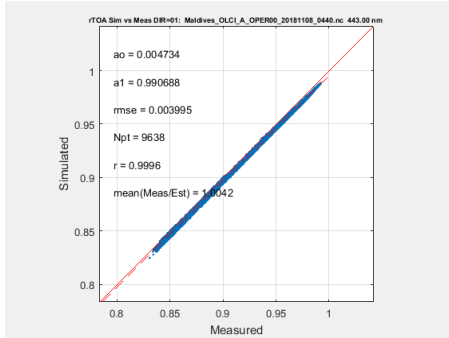
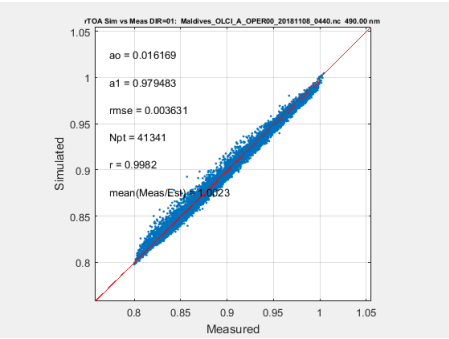	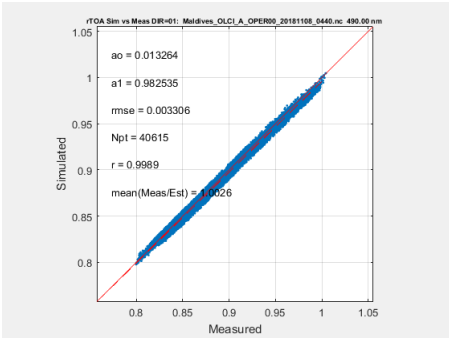	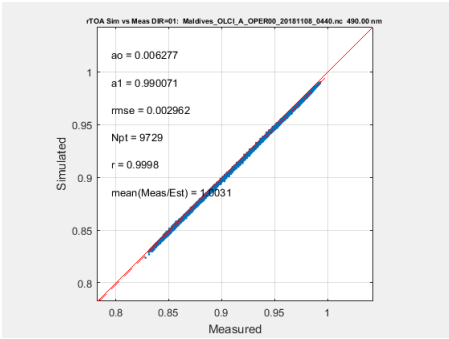	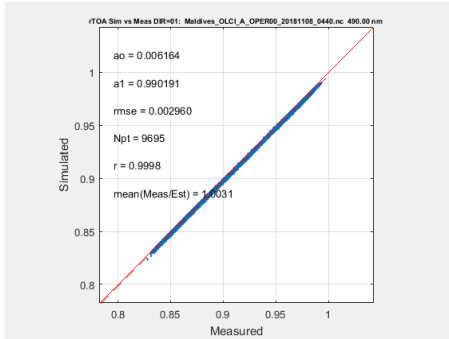

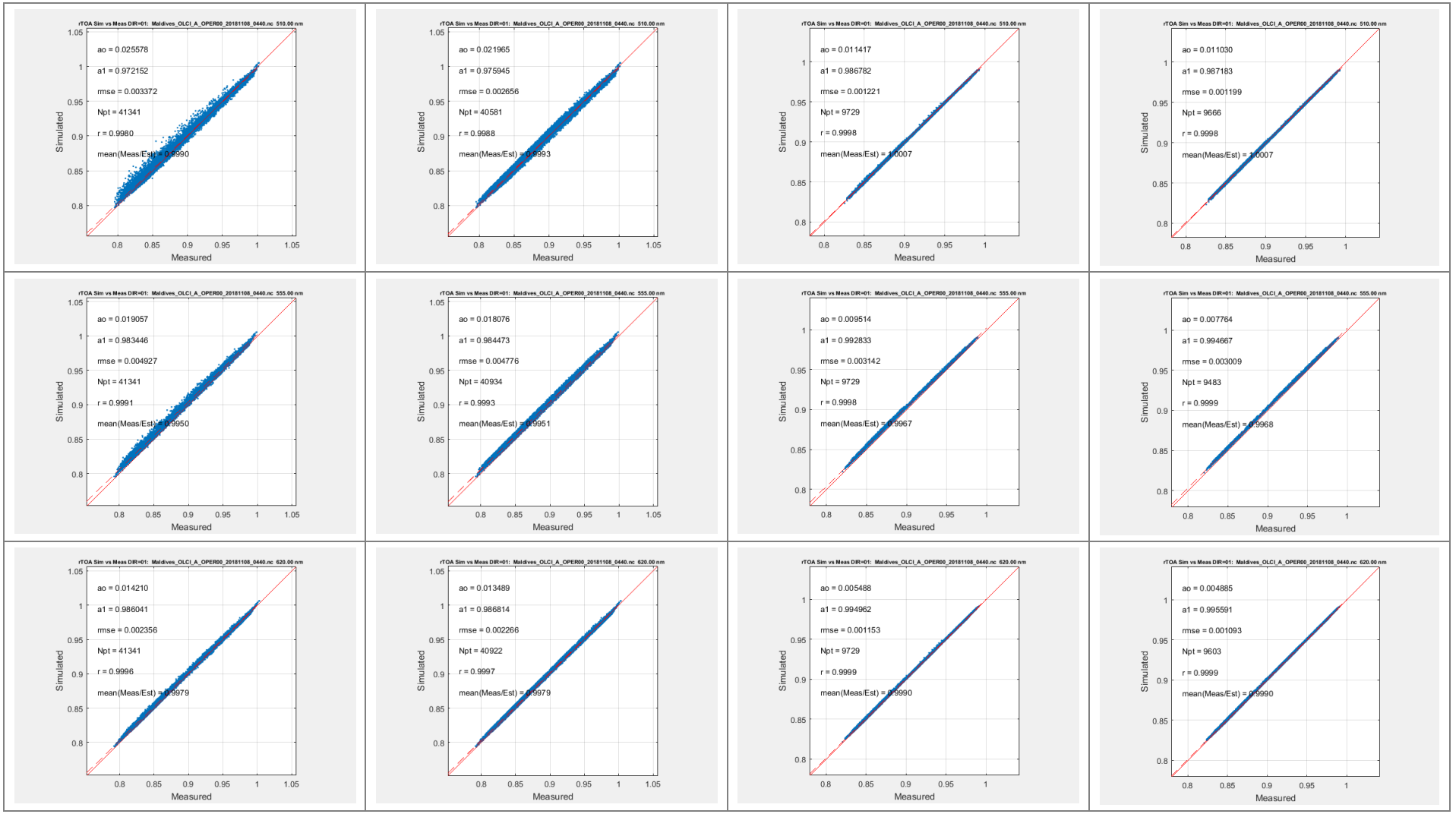

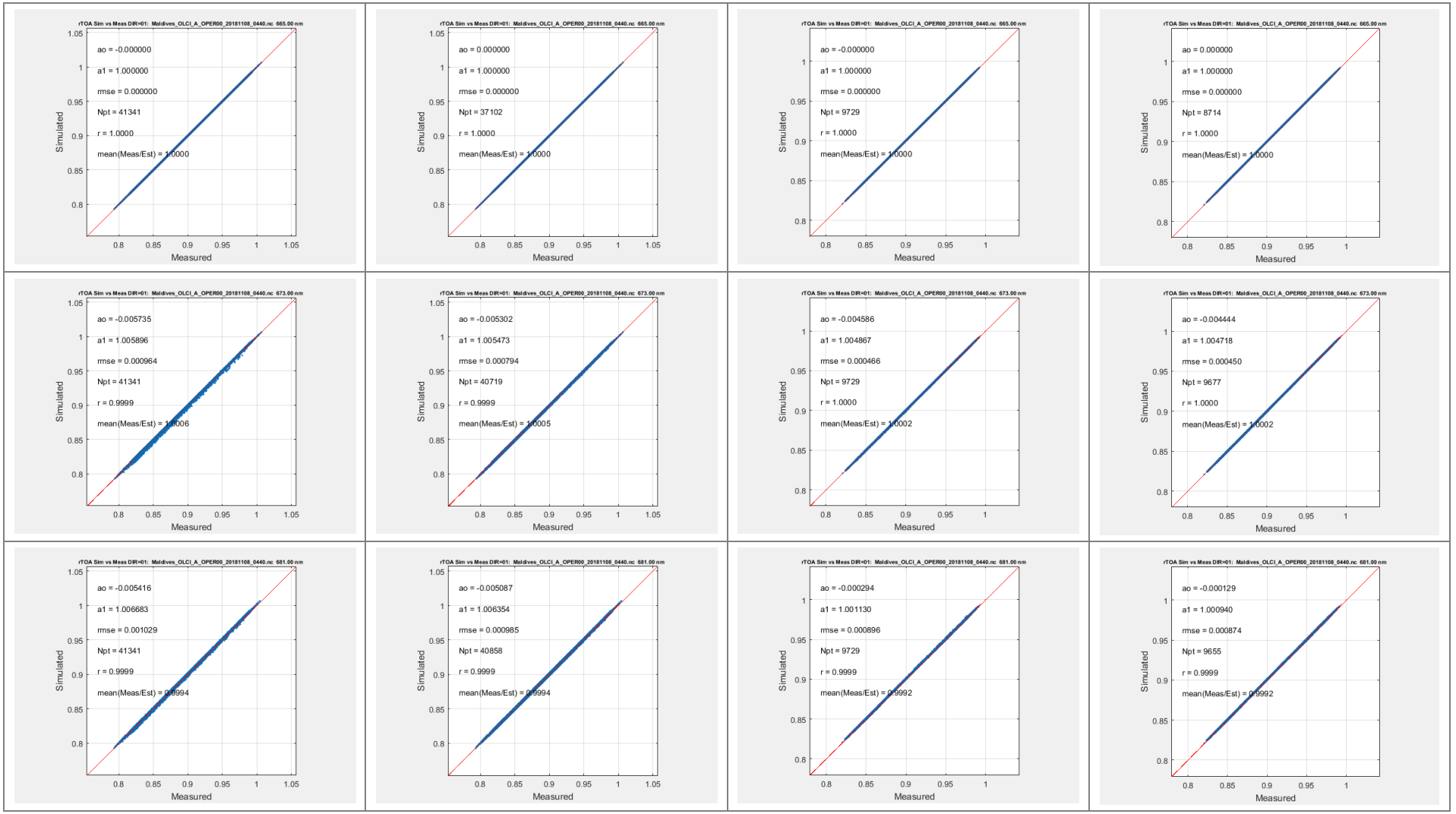

List of the Figures

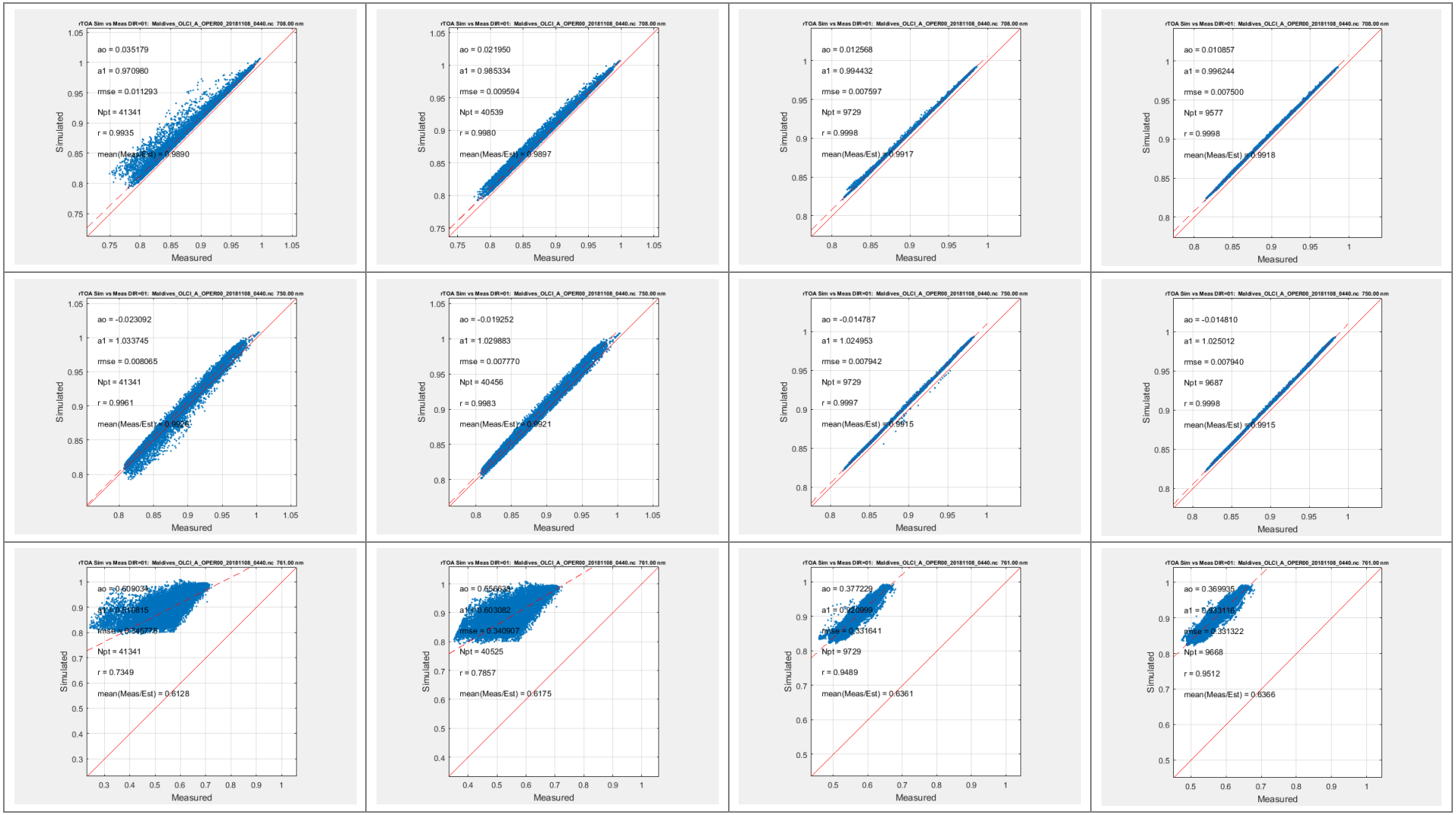

List of the Figures

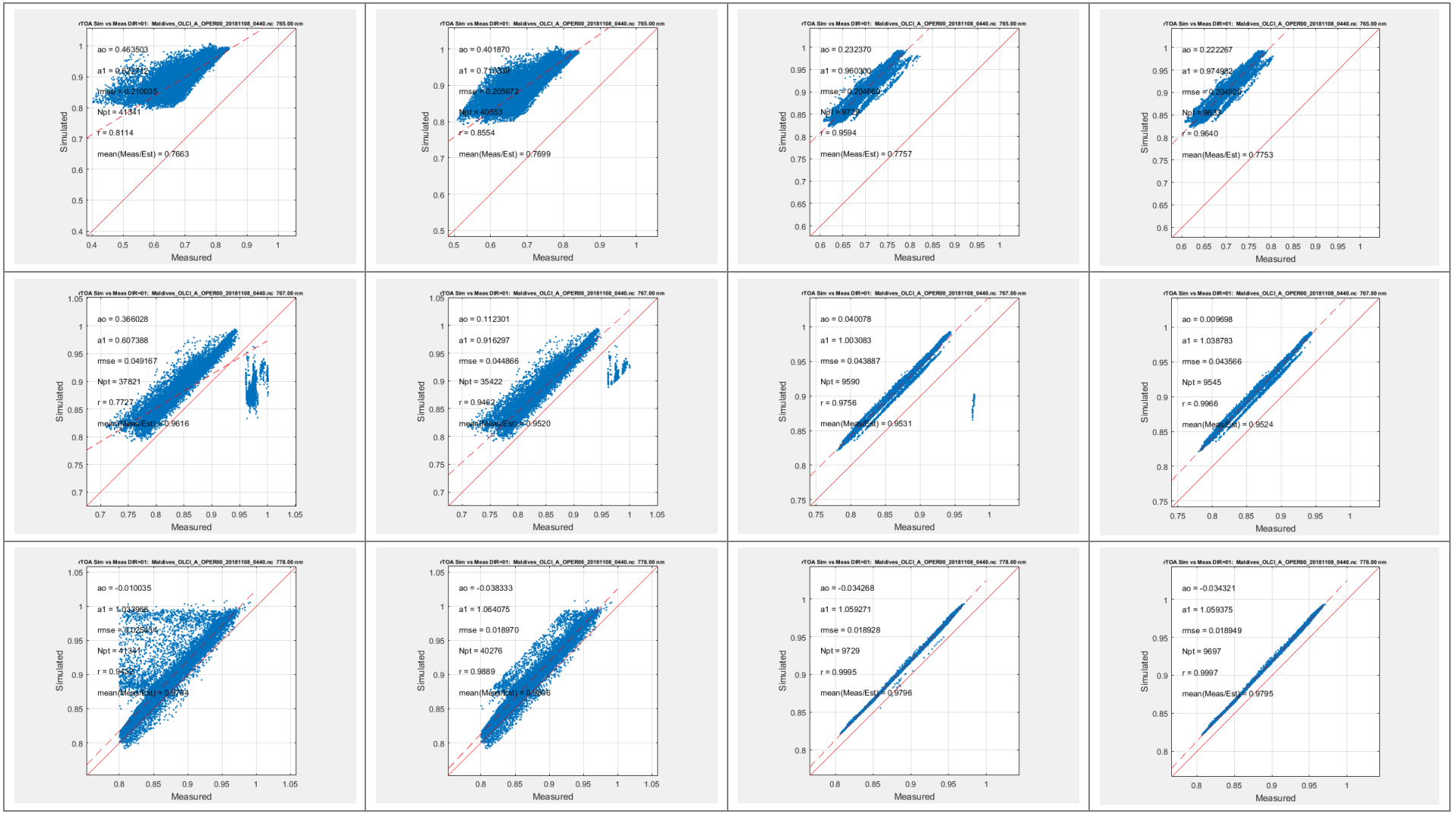

List of the Figures

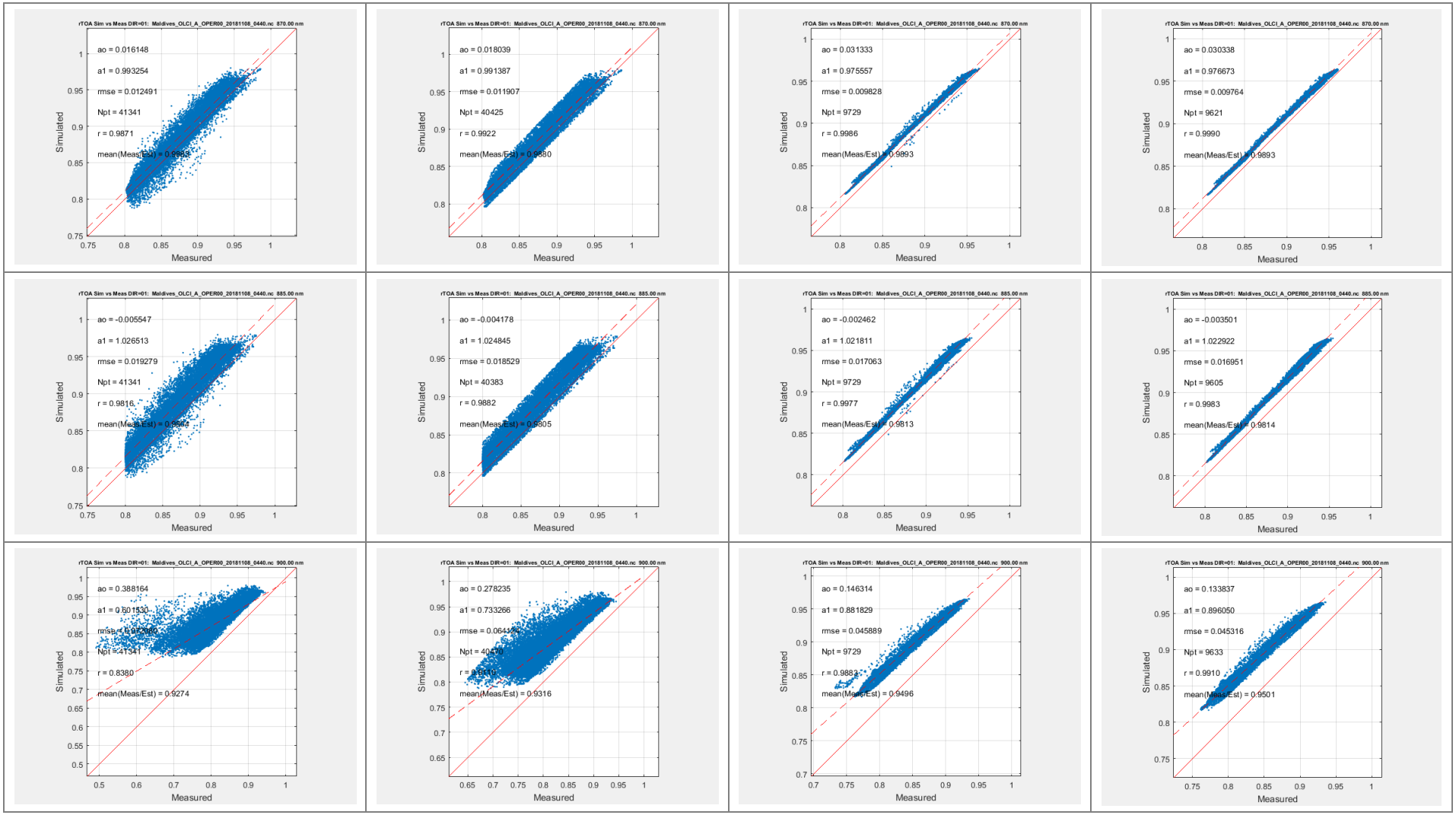

List of the Figures

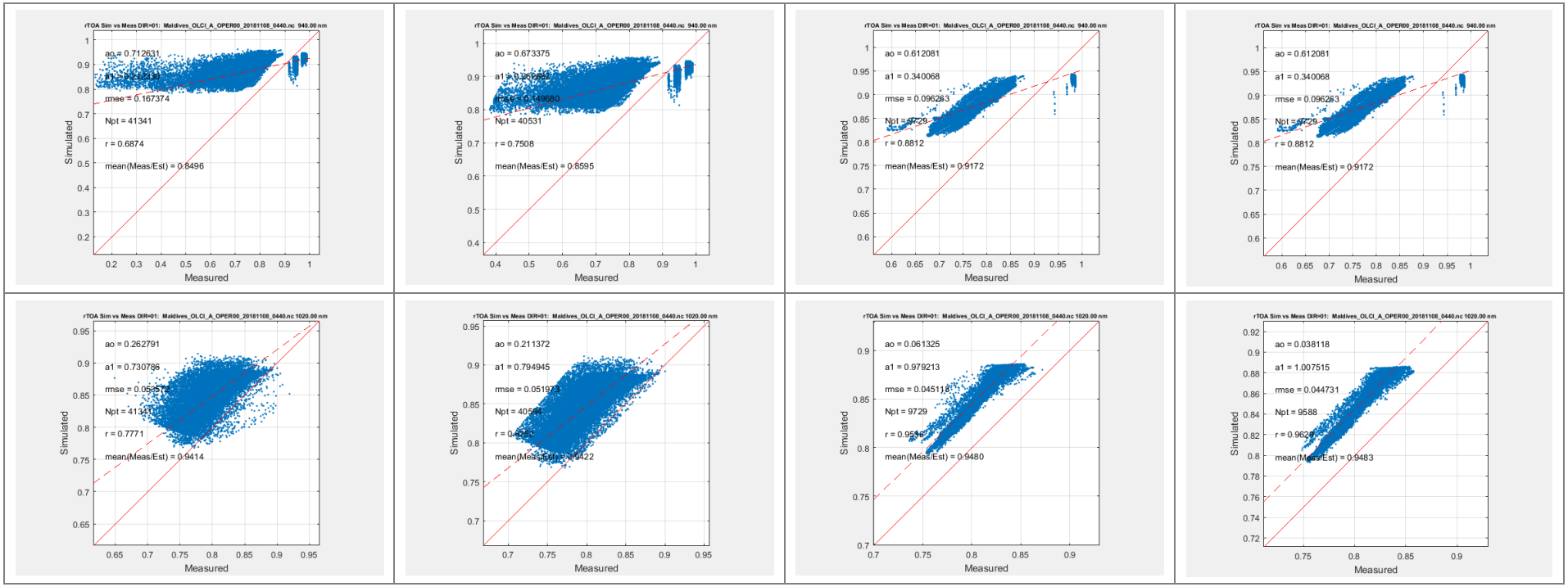

6.2 For a temporal series analysis

6.2.1 Results for Case 4 (filtering of the outliers at 3 sigma and DCC pixels selected if they are in a 3 km2 DCC area)

The temporal evolution of the ratio of measured to simulated reflectance is presented in the figure below for all spectral bands.

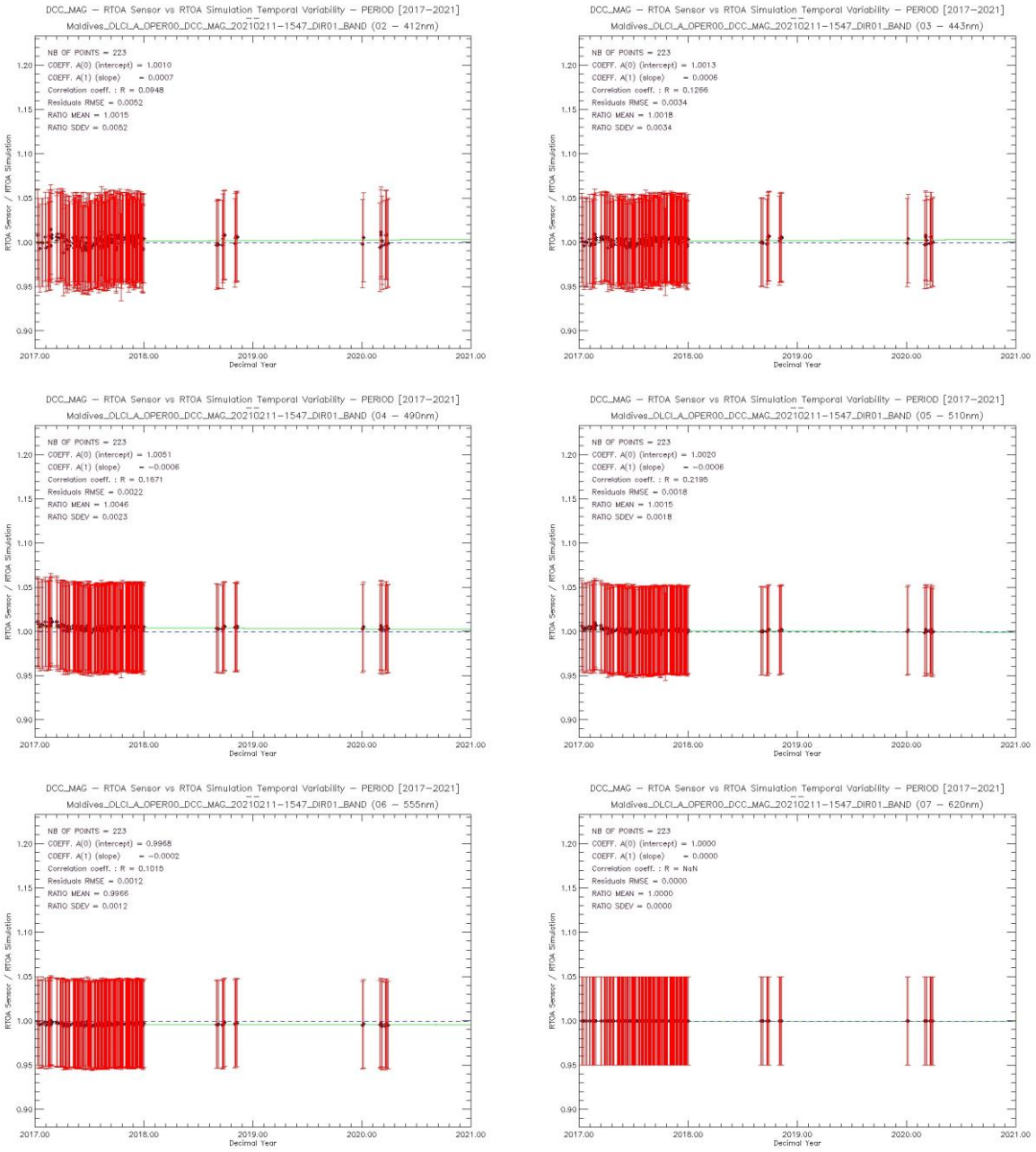

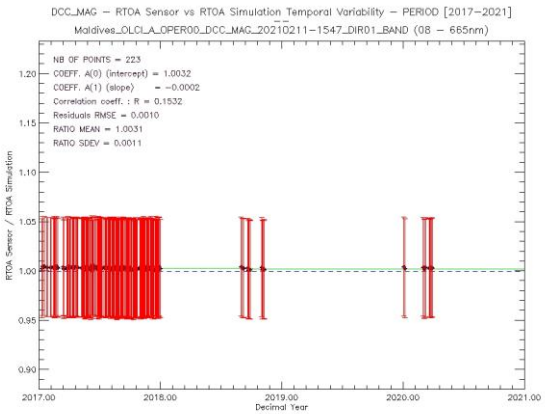

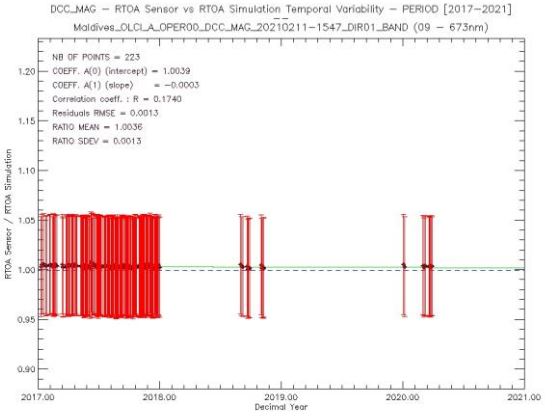

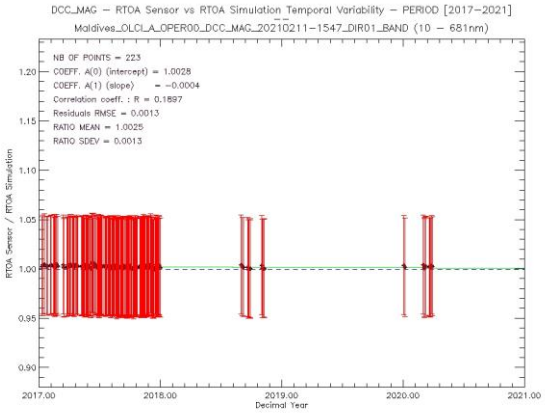

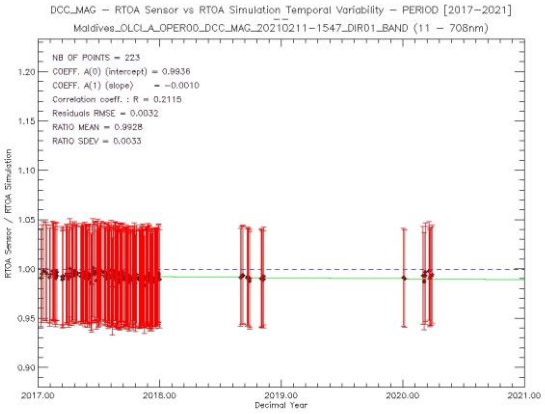

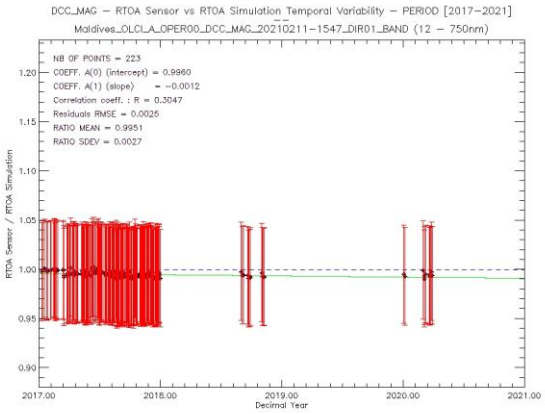

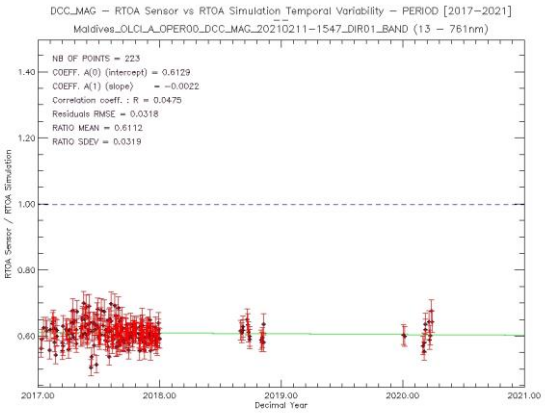

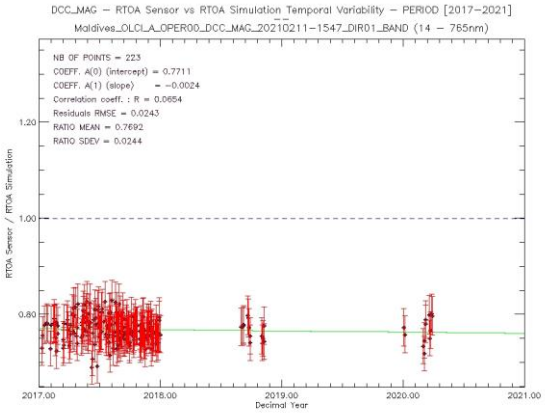

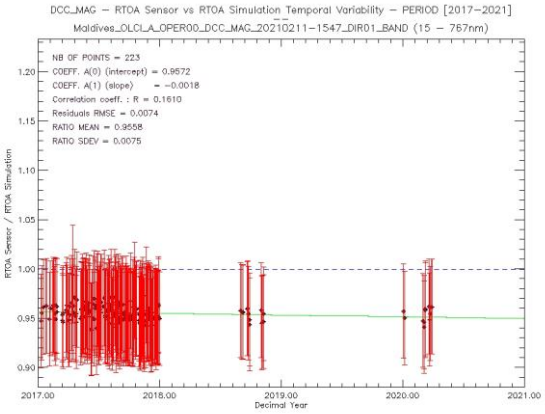

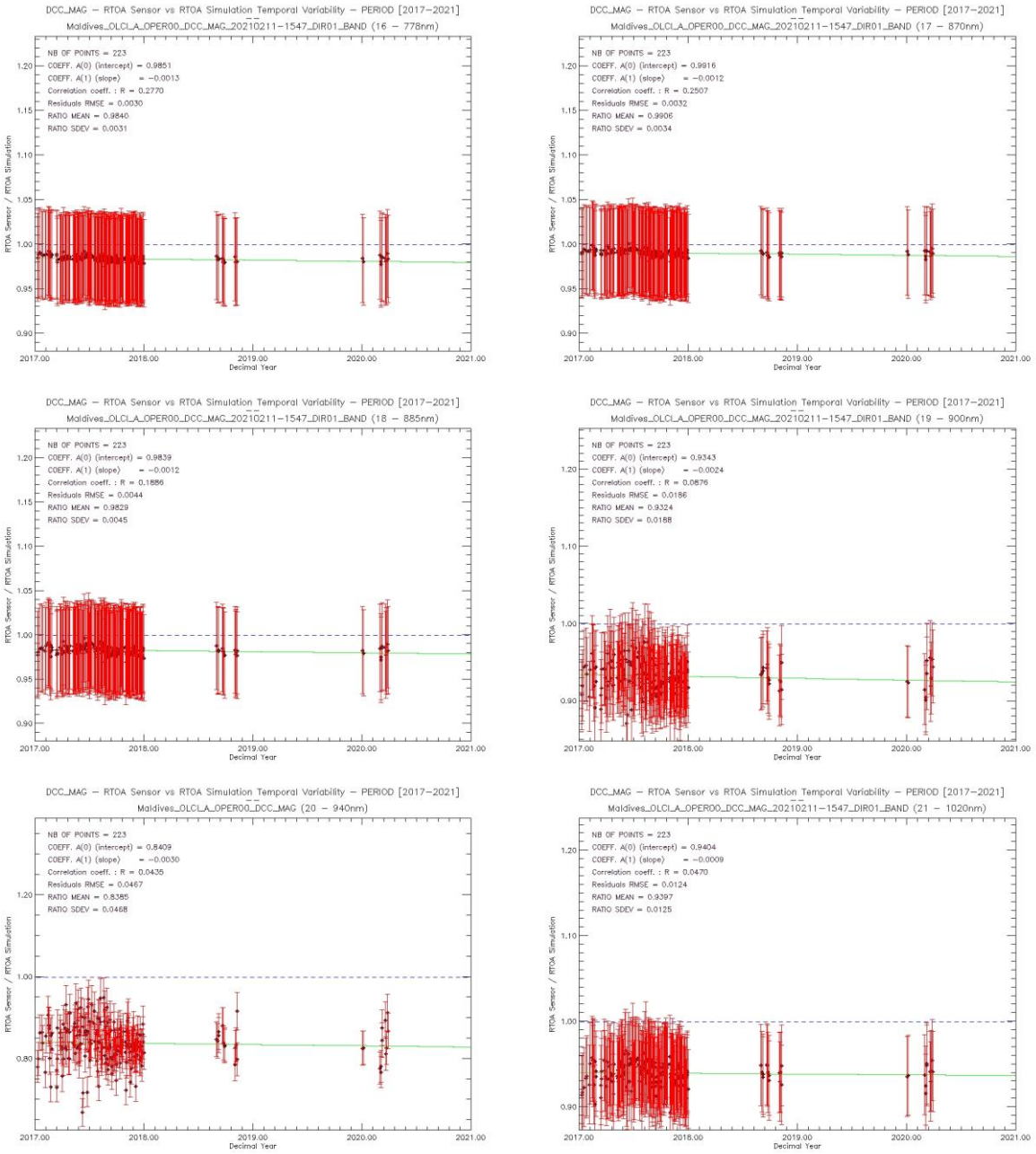

Figure 6-3: Temporal variability of the measured to simulation reflectance ratio over DCC

Table 6-1: Statistics of the monitoring

Band center	400	412.5	442.5	490	510	560	620	665	673.75	681.25	708.75
Ao		0.000728	0.000637	-0.000561	-0.000598	-0.000176		-0.000239	-0.000332	-0.000373	-0.001018
A1		1.00096	1.00133	1.00509	1.00199	0.99676		1.00325	1.0039	1.00278	0.993578
Rmse		0.005174	0.003374	0.002239	0.001799	0.001167		0.001041	0.001269	0.001304	0.003184
R		0.094803	0.126616	0.167146	0.219533	0.101479		0.153201	0.173961	0.189707	0.211468
Npt		223	223	223	223	223	223	223	223	223	223
Std		0.005209	0.003409	0.002276	0.001848	0.001175	0.000000	0.001056	0.001292	0.001331	0.003265
mean		1.00155	1.00184	1.00463	1.00151	0.996618	1	1.00306	1.00364	1.00248	0.99276

	753.75	761.25	764.375	767.5	778.75	865	885	900	940	1020
Ao	-0.001193	-0.002238	-0.002352	-0.001788	-0.001278	-0.001242	-0.001250	-0.002425	-0.003003	-0.000867
A1	0.996038	0.612948	0.771098	0.957221	0.985057	0.991565	0.983872	0.934331	0.840925	0.940361
Rmse	0.002523	0.031826	0.024288	0.007412	0.003000	0.003243	0.004402	0.018649	0.046665	0.012443
R	0.304732	0.047512	0.065360	0.161040	0.276989	0.250690	0.188624	0.087617	0.043492	0.047049
Npt	223	223	223	223	223	223	223	223	223	223
Std	0.002655	0.031934	0.024395	0.007527	0.003129	0.003358	0.004493	0.018763	0.046815	0.012484
mean	0.99508	0.611151	0.76921	0.955785	0.98403	0.990568	0.982869	0.932384	0.838514	0.939665

6.2.2 Conclusion

The possible use of deep convective clouds (DCCs) for the monitoring of sensor radiometry channels is illustrated using OLCI/S3A measurements for all bands except band 1 (due do RTM limitations) and bands located in O_2 and H_20 absorption.

Case 4 is retained as nominal for the method implementation.

7 Sensitivity study

Main contributors of uncertainties introduced in our implementation could come from:

1. Cloud effective radius: an error of 10 µm is considered in the error analysis
2. Microphysical properties model: Baum mixture of particles is compared to Yang ice crystal parameterization
3. Cloud top height: the uncertainty in the cloud altitude leads to an uncertainty of the Rayleigh scattering contribution above the clouds. In the simulations, cloud top altitude is decreased to 10 km.
4. A sensitivity to different parameters of the simulation has been conducted. The tests are performed using the RTM Libradtran with different cloud and atmosphere parameters. The wavelength of the reference band is also assessed.
5. Aerosol scattering affects with higher aerosol load is assessed.
6. Reference band choice Is also assessed

Tests are based using the same pixel on the acquisition 08/11/2018. The table below reports the change in the parameters. Last row reports the rmse.

Table 7-1: Parameters used for simulations

Test Number	1	2	3	4	5	6	7	8	9
	reference								
Top Height Cloud (km)	15	15	10	15	15	15	15	15	15
Bottom Height Cloud (km)	1	1	1	1	1	1	1	1	1
Effective Radius µ(m)	20	20	20	30	20	40	25	20	20
LWC (g.m-3)	0.15	0.15	0.15	0.15	0.15	0.15	0.15	0.1	0.15
AOT	0.05	0.08	0.05	0.05	0.05	0.05	0.05	0.05	0.05
Cloud model	Baum	Baum	Baum	Baum	yang	Baum	Baum	Baum	Baum
Reference band (nm)	620	620	620	620	620	620	620	620	665
rmse	0.0046	0.0046	0.0046	0.0029	0.005	0.0034	0.0038	0.0043	0.0041

The spectral variability of the results is shown on Figure 7-1 and details on the following figure which are zoomed to make the difference between simulations visible.

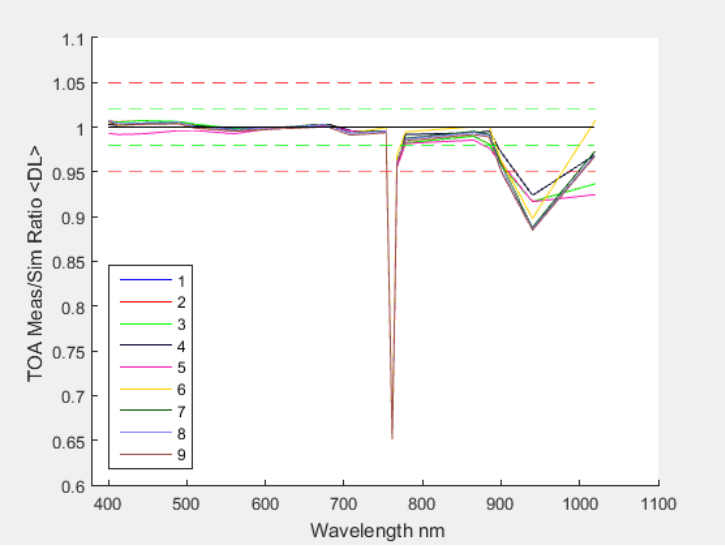

Figure 7-1: Measured to Simulated ratio of OLCI TOA reflectance using DCC target. Numbers in the legend correspond to the case described in the table above.

A detail of the figure for ratio comprised between 0.95 and 1.05 is represented below. The pink curve is the simulation with the Yang model.

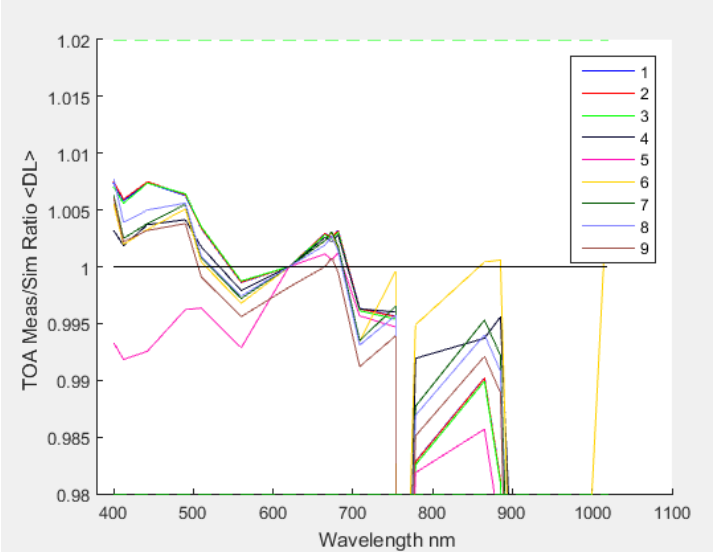

Figure 7-2: Measured to Simulated ratio of OLCI TOA reflectance using DCC target. Numbers in the legend correspond to the case described in the table above.

For the spectral bands located before 500 nm, the differences in simulations can be observed on the figure below.

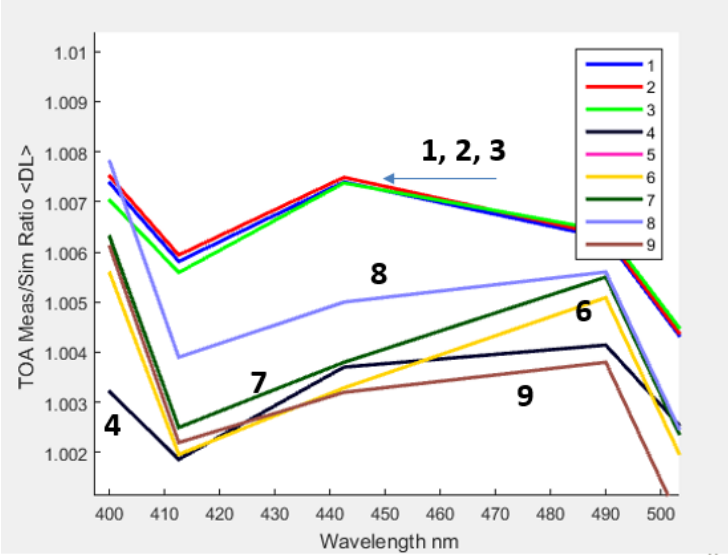

Figure 7-3: Measured to Simulated ratio of OLCI TOA reflectance using DCC target for bands located before 500 nm. Numbers in the legend correspond to the case described in the table above.

- End of the document -